Numerical computations of flow in rotating ducts with strong curvature

F. Papa
Chemical Engineering Department, University of Toledo, Ohio, USA
K. Vaidyanathan
Federal-Mogul Co., Ann Arbor, Michigan, USA
T.G. Keith, Jr
Mechanical Engineering Department, University of Toledo, Ohio, USA, and
K.J. DeWitt
Chemical Engineering Department, University of Toledo, Ohio, USA

Received September 1999
Revised May 2000
Accepted May 2000

Keywords *Fluids, Laminar flow, Numerical methods, Rotating flows*

Abstract *The artificial compressibility method is used to analyze internal flows in rotating ducts having strong curvature. This study was concerned with the laminar flow of an incompressible Newtonian fluid having constant viscosity in circular and square ducts with a 90° bend. The emphasis of the present simulation is to determine the effect of rotation and through-flow rate on the fluid physics and friction characteristics in the straight channel and in the curved geometric regions. The Reynolds numbers ranged from 100 to 790 and the Rossby numbers from 0 to 0.4. Coriolis forces arising from rotation produce a non-symmetric secondary flow in the bend that increases the loss coefficient as compared with the values for non-rotation. In addition, the wall friction losses in the straight outlet section are increased, and both effects are directly proportional to the Rossby number.*

Nomenclature

D	= reference length
$\hat{D}$	= transient vector
$\hat{E}_C, \hat{F}_C, \hat{G}_C$	= convective vectors
$\hat{E}_V, \hat{F}_V, \hat{G}_V$	= viscous vectors
J	= Jacobian
P	= pressure
Re	= Reynolds number
Ro	= Rossby number
x, y, z	= Cartesian coordinate axes
u, v, w	= Cartesian velocity components
t	= time
$\overline{W}$	= average velocity over the cross section
U, V, W	= contravariant velocities

Greek symbols

ξ, η, ζ	= generalized coordinate axes
ξ_i, η_i, ζ_i	= metrics of the transformation
μ	= dynamic viscosity
ρ	= density
τ_{ij}	= shear stress
Ω	= rate of rotation

The authors wish to thank The Federal-Mogul Company for providing technical and financial support of this work.

International Journal of Numerical Methods for Heat & Fluid Flow, Vol. 10 No. 5, 2000, pp. 541-556.

Introduction

Flows in rotating ducts occur in numerous and diverse industrial processes. These include flows in cooling passages of turbine blades, flows in lubrication systems in car engines and flows in centrifugal compressors. Such flow cases have strong secondary flows due to the presence of Coriolis forces.

The effects of rotation on the hydrodynamics of internal flows have considerable practical implications in the design of turbine-blade cooling passages. The cooling arrangements in modern gas turbine blades commonly entail the circulation of "cool" air through roughly square, serpentine, cooling passages in the blade interior. The very tight bend that terminates each straight section of the passage causes secondary flow, and the flow is further complicated by the blade rotation which induces a significant Coriolis force on the flow.

The development of secondary flows in the pressure-driven flow of a fluid through a duct that is rotating has been studied in the past. The earliest work on this subject consisted of theoretical investigations of the weak-rotation (Rossby number close to zero) case for laminar flow in circular straight pipes. Barua (1955), by using a perturbation approach, showed that for weak rotations the secondary flow consisted of a counter-rotating-double-vortex configuration similar to that which occurs in a stationary curved pipe. Benton and Boyer (1966), Mori and Nakayama (1968), and Ito and Nanbu (1971) have also attempted theoretical analyses of fully-developed laminar flow by assuming that the flow may be treated as a central core region together with a relatively thin boundary layer region in the immediate vicinity of the wall.

Only a limited amount of experimental data is available for comparison with theory. Measurements of the axial velocity in two-dimensional flows in rotating ducts have been reported by Moore (1967) and by Johnston *et al.* (1972). Experimental results for axial velocity have also been reported for three-dimensional flows (Moore, 1973; Hill and Moon, 1962). However, no experimental measurements are available in the literature for secondary flows in rotating ducts with strong curvature.

The present work is a computational study of laminar flow through a rotating duct with parallel rotation at the inlet and orthogonal rotation at the outlet. The purpose of this work is to study the flow in rotating ducts with 90° bends. The flow in both square and circular ducts was studied for different Reynolds and Rossby numbers.

The governing partial differential equations are solved using the finite-difference procedure of Vaidyanathan (1998) adapted to a non-inertial frame of reference. A third-order upwind scheme was used for the convective terms and second-order central differences were used for the viscous terms.

Governing equations and the model problem

Figures 1(a) and 1(b) show, respectively, a square and circular duct having 90° bends and which are rotating about the entry flow axis. In both cases the straight flow sections before and after the bend were set to a length of five

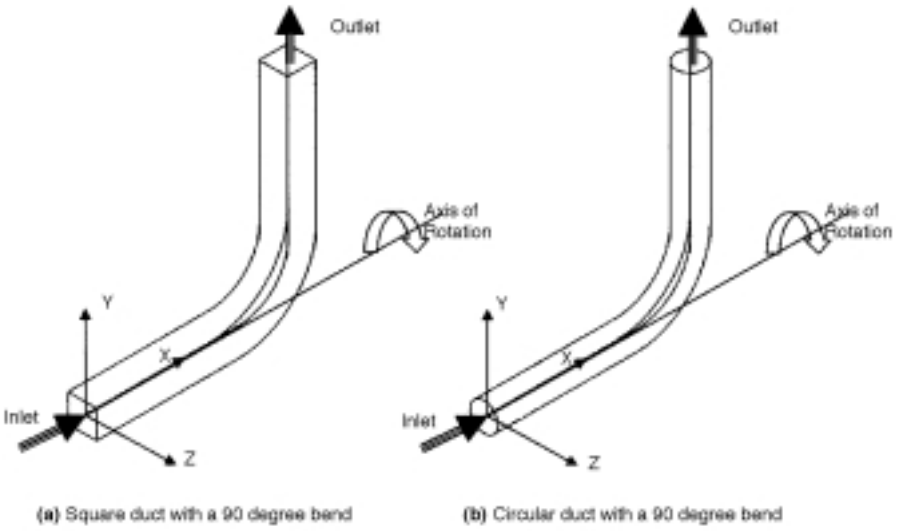

Figure 1.
Square and circular ducts with a 90° bend

times the duct diameter. The radius of curvature of the inner wall in the curved section is 1.8 times its diameter. The flow field considered is laminar and steady, and the fluid is incompressible and Newtonian with constant viscosity.

The circular or square duct under rotation represents a non-inertial frame of reference because the ducts are accelerating and therefore forces are acting on them. The governing equations used in the flow modeling must be modified in a way that will consider these new forces due to rotation, which comprise centripetal and Coriolis forces. The governing equations, with respect to the x, y, z coordinate system, are

Continuity

$$\frac{\partial u}{\partial x}+\frac{\partial v}{\partial y}+\frac{\partial w}{\partial z}=0 \tag{1}$$

Momentum
x-component

$$\rho\left(u\frac{\partial u}{\partial x}+v\frac{\partial u}{\partial y}+w\frac{\partial u}{\partial z}\right)=-\frac{\partial P}{\partial x}+\mu\left(\frac{\partial^2 u}{\partial x^2}+\frac{\partial^2 u}{\partial y^2}+\frac{\partial^2 u}{\partial z^2}\right) \tag{2}$$

y-component

$$\rho\left(u\frac{\partial v}{\partial x}+v\frac{\partial v}{\partial y}+w\frac{\partial v}{\partial z}\right)=-\frac{\partial P}{\partial y}+\mu\left(\frac{\partial^2 v}{\partial x^2}+\frac{\partial^2 v}{\partial y^2}+\frac{\partial^2 v}{\partial z^2}\right)+2\Omega w \tag{3}$$

z-component

$$\rho\left(u\frac{\partial w}{\partial x}+v\frac{\partial w}{\partial y}+w\frac{\partial w}{\partial z}\right)=-\frac{\partial P}{\partial z}+\mu\left(\frac{\partial^2 w}{\partial x^2}+\frac{\partial^2 w}{\partial y^2}+\frac{\partial^2 w}{\partial z^2}\right)-2\Omega v \tag{4}$$

Here, u, v, and w are the velocity components in the x, y, and z directions, respectively. The quantity P is the modified pressure and Ω is the magnitude of the rotation vector about the x-direction.

The modified pressure is defined as

$$P = p + \rho\Phi \tag{5}$$

where p is the static pressure term and Φ is the potential of the centripetal term.

Equations (1)-(4) are written in dimensionless terms using a reference length and reference velocity. The reference velocity used was the average velocity over a cross-section, $\overline{W}$.

The reference length for the circular duct was the diameter and for the square duct was the side length, both designated by D. The dimensionless quantities obtained are

$$x^* = \frac{x}{D} \quad u^* = \frac{u}{\overline{W}} \quad P^* = \frac{P}{\rho\overline{W}^2}$$
$$y^* = \frac{y}{D} \quad v^* = \frac{v}{\overline{W}} \quad t^* = \frac{t\overline{W}}{D}$$
$$z^* = \frac{z}{D} \quad w^* = \frac{w}{\overline{W}} \quad \Omega^* = \frac{\Omega D}{\overline{W}}$$

Using these dimensionless quantities, the dimensionless form of equations (1)-(4) was obtained.

The dimensionless governing equations contain two parameters: the Reynolds number (Re), which is the ratio of the inertial force to the viscous force, and the Rossby number (Ro), which is the ratio of the Coriolis force to the inertial force:

$$Re = \frac{\rho\overline{W}D}{\mu} \qquad Ro = \frac{2\Omega D}{\overline{W}} \tag{6}$$

The governing equations, as written, can only be used to solve problems in a cartesian coordinate system.

These equations were transformed to a generalized system and are written in the strong conservation law form as suggested by Viviand (1974) as

$$\frac{\partial}{\partial\xi}(\hat{E}_c - \hat{E}_v) + \frac{\partial}{\partial\eta}(\hat{F}_c - \hat{F}_v) + \frac{\partial}{\partial\zeta}(\hat{G}_c - \hat{G}_v) = \hat{S} \tag{7}$$

where the convective vectors are

$$\hat{E}_C = \frac{1}{J}\begin{bmatrix} U \\ u^*U + P^*\xi_X \\ v^*U + P^*\xi_Y \\ w^*U + P^*\xi_Z \end{bmatrix} \quad \hat{F}_C = \frac{1}{J}\begin{bmatrix} V \\ u^*V + P^*\eta_X \\ v^*V + P^*\eta_Y \\ w^*W + P^*\eta_Z \end{bmatrix} \quad \hat{G}_C = \frac{1}{J}\begin{bmatrix} W \\ u^*W + P^*\zeta_X \\ v^*W + P^*\zeta_Y \\ w^*W + P^*\zeta_Z \end{bmatrix} \tag{8}$$

and U, V, W are

$$\begin{aligned} U &= \xi_x u^* + \xi_y v^* + \xi_z w^* \\ V &= \eta_x u^* + \eta_y v^* + \eta_z w^* \\ W &= \zeta_x u^* + \zeta_y v^* + \zeta_z w^* \end{aligned} \tag{9}$$

The quantity J is the Jacobian of the transformation defined as the determinant of the Jacobian matrix:

$$J = \frac{(x^*, y^*, z^*)}{(\xi, \eta, \zeta)} \tag{10}$$

The viscous vectors are defined as

$$\hat{E}_V = \frac{1}{J}\begin{bmatrix} 0 \\ \xi_X\tau_{XX} + \xi_Y\tau_{XY} + \xi_Z\tau_{XZ} \\ \xi_X\tau_{XY} + \xi_Y\tau_{YY} + \xi_Z\tau_{YZ} \\ \xi_X\tau_{XZ} + \xi_Y\tau_{YZ} + \xi_Z\tau_{ZZ} \end{bmatrix} \quad \hat{F}_V = \frac{1}{J}\begin{bmatrix} 0 \\ \eta_X\tau_{XX} + \eta_Y\tau_{XY} + \eta_Z\tau_{XZ} \\ \eta_X\tau_{XY} + \eta_Y\tau_{YY} + \eta_Z\tau_{YZ} \\ \eta_X\tau_{XZ} + \eta_Y\tau_{YZ} + \eta_Z\tau_{ZZ} \end{bmatrix}$$

$$\hat{G}_V = \frac{1}{J}\begin{bmatrix} 0 \\ \zeta_X\tau_{XX} + \zeta_Y\tau_{XY} + \zeta_Z\tau_{XZ} \\ \zeta_X\tau_{XY} + \zeta_Y\tau_{YY} + \zeta_Z\tau_{YZ} \\ \zeta_X\tau_{XZ} + \zeta_Y\tau_{YZ} + \zeta_Z\tau_{ZZ} \end{bmatrix} \tag{11}$$

and τ_{XX}, τ_{YY}, τ_{ZZ}, τ_{XY}, τ_{XZ}, τ_{YZ} are

$$\begin{aligned} \tau_{XX} &= \frac{2}{Re}\left[\xi_X u^*_\xi + \eta_X u^*_\eta + \zeta_X u^*_\zeta\right] \\ \tau_{YY} &= \frac{2}{Re}\left[\xi_Y v^*_\xi + \eta_Y v^*_\eta + \zeta_Y v^*_\zeta\right] \\ \tau_{ZZ} &= \frac{2}{Re}\left[\xi_Z w^*_\xi + \eta_Z w^*_\eta + \zeta_Z w^*_\zeta\right] \\ \tau_{XY} &= \frac{1}{Re}\left[\xi_Y u^*_\xi + \eta_Y u^*_\eta + \zeta_Y u^*_\zeta + \xi_X v^*_\xi + \eta_X v^*_\eta + \zeta_X v^*_\zeta\right] \\ \tau_{YZ} &= \frac{1}{Re}\left[\xi_Z v^*_\xi + \eta_Z v^*_\eta + \zeta_Z v^*_\zeta + \xi_Y w^*_\xi + \eta_Y w^*_\eta + \zeta_Y w^*_\zeta\right] \\ \tau_{XZ} &= \frac{1}{Re}\left[\xi_X w^*_\xi + \eta_X w^*_\eta + \zeta_X w^*_\zeta + \xi_Z u^*_\xi + \eta_Z u^*_\eta + \zeta_Z u^*_\zeta\right] \end{aligned}$$

The new terms due to the Coriolis forces are included in the governing equation as a source term:

$$\hat{\mathrm{S}} = \frac{1}{\mathrm{J}} \begin{bmatrix} 0 \\ 0 \\ \mathrm{Row}^* \\ -\mathrm{Rov}^* \end{bmatrix} \tag{12}$$

Numerical method

Equation (7) was solved using a finite difference numerical approach. The primary difficulty in computing a solution to equation (7) is because the fluid is incompressible, and it is therefore necessary to find a method to link changes in the velocity field to changes in the pressure field. The method suggested by Chorin (1967), known as the artificial compressibility method, was used to link the continuity equation with the momentum equation. Using this formulation, an artificial term, the time derivative of the pressure, is added to the continuity equation. The unsteady terms are also added to the momentum equation to allow the program to iterate on time until the steady state solution is obtained. Equation (7) was modified in a way that allowed the use of the artificial compressibility method, but it should be noticed that when the steady state solution is obtained, equation (13) reduces to equation (7).

$$\frac{\partial}{\partial \mathrm{t}}(\hat{\mathrm{D}}) + \frac{\partial}{\partial \xi}(\hat{\mathrm{E}}_{\mathrm{c}} - \hat{\mathrm{E}}_{\mathrm{v}}) + \frac{\partial}{\partial \eta}(\hat{\mathrm{F}}_{\mathrm{c}} - \hat{\mathrm{F}}_{\mathrm{v}}) + \frac{\partial}{\partial \zeta}(\hat{\mathrm{G}}_{\mathrm{c}} - \hat{\mathrm{G}}_{\mathrm{v}}) = \hat{\mathrm{S}} \tag{13}$$

where

$$\hat{\mathrm{D}} = \begin{bmatrix} \mathrm{P}^*/\beta \\ \mathrm{u}^* \\ \mathrm{v}^* \\ \mathrm{w}^* \end{bmatrix}$$

and β is an artificial compressibility constant.

Equation (13) contains three types of terms: first-order spatial derivative terms; second-order derivative terms; and cross-derivative terms. The first-order spatial derivative arising from the convective vector was represented using a third-order upwind scheme, and the other derivatives were represented using a central difference scheme.

Boundary conditions are needed at the inlet, exit and the wall. At the inlet, the velocity distribution is specified as a fully developed flow. At the outlet, pressure and velocity are extrapolated from internal nodes. At the walls, no slip and no penetration are assumed. The pressure boundary condition used at the wall is the boundary layer approximation in a rotating frame of reference, therefore the modified pressure gradient normal to the wall is assumed to be zero. All boundaries were coupled and subjected to implicit treatment. It has been shown

by Chen (1990) that an implicit boundary condition treatment permits the use of large time steps, allowing the algorithm to converge to the asymptotic steady state much faster than schemes that use explicit boundary conditions.

Results and discussion

Multiple simulations were performed in this work. Table I summarize the cases solved with the code and the grid definition used for each case. Different grid sizes were used in this study, and some significant aspects were noticed. The coarsest grid used was $51 \times 21 \times 21$ (nearly 23,000 grid points) nodes in the streamwise, normal and radial directions, respectively. It was found that solutions for low Reynolds numbers converged rapidly. Solutions for higher Reynolds numbers required a finer mesh. This was accomplished using grids with $71 \times 31 \times 31$ (68,000 grid points) nodes and $101 \times 41 \times 41$ (170,000 grid points) nodes in the streamwise, normal and radial directions, respectively.

Figure 2 shows the velocity profiles obtained at different angular locations along the bend for the square duct. These profiles are compared with the numerical results of Yeo *et al.* (1991) and the experimental data of Humphrey *et al.* (1977) along the center-line at $z = 0$. The Reynolds number was 790 and there is no rotation. The grid definition used in this comparison was $71 \times 31 \times 31$, and good agreement was obtained among all three studies at the 0° and 90° planes, with lesser agreement with the experimental data along the 30° and 60° planes.

Several solutions were obtained for the 90° bend with a square cross-section for different grid resolutions, at the same Reynolds and Rossby numbers, and results that are nearly independent of the grid resolution were obtained. The

Duct type	Re	Ro	Grid definition
Square	100	0.0	$51 \times 21 \times 21$
Square	300	0.0	$51 \times 21 \times 21$
Square	500	0.4	$51 \times 21 \times 21$
		0.2	
		0.0	
Square	790	0.0	$51 \times 21 \times 21$
Square	100	0.4	$71 \times 31 \times 31$
		0.2	
		0.0	
Square	300	0.4	$71 \times 31 \times 31$
Square	500	0.4	$71 \times 31 \times 31$
Square	790	0.0	$71 \times 31 \times 31$
		0.2	
		0.4	
Square	100	0.0	$101 \times 41 \times 41$
Circular	100	0.0	$71 \times 31 \times 31$
		0.2	
		0.4	
Circular	790	0.0	$71 \times 31 \times 31$
		0.4	

Table I. Summary of the cases solved in this work

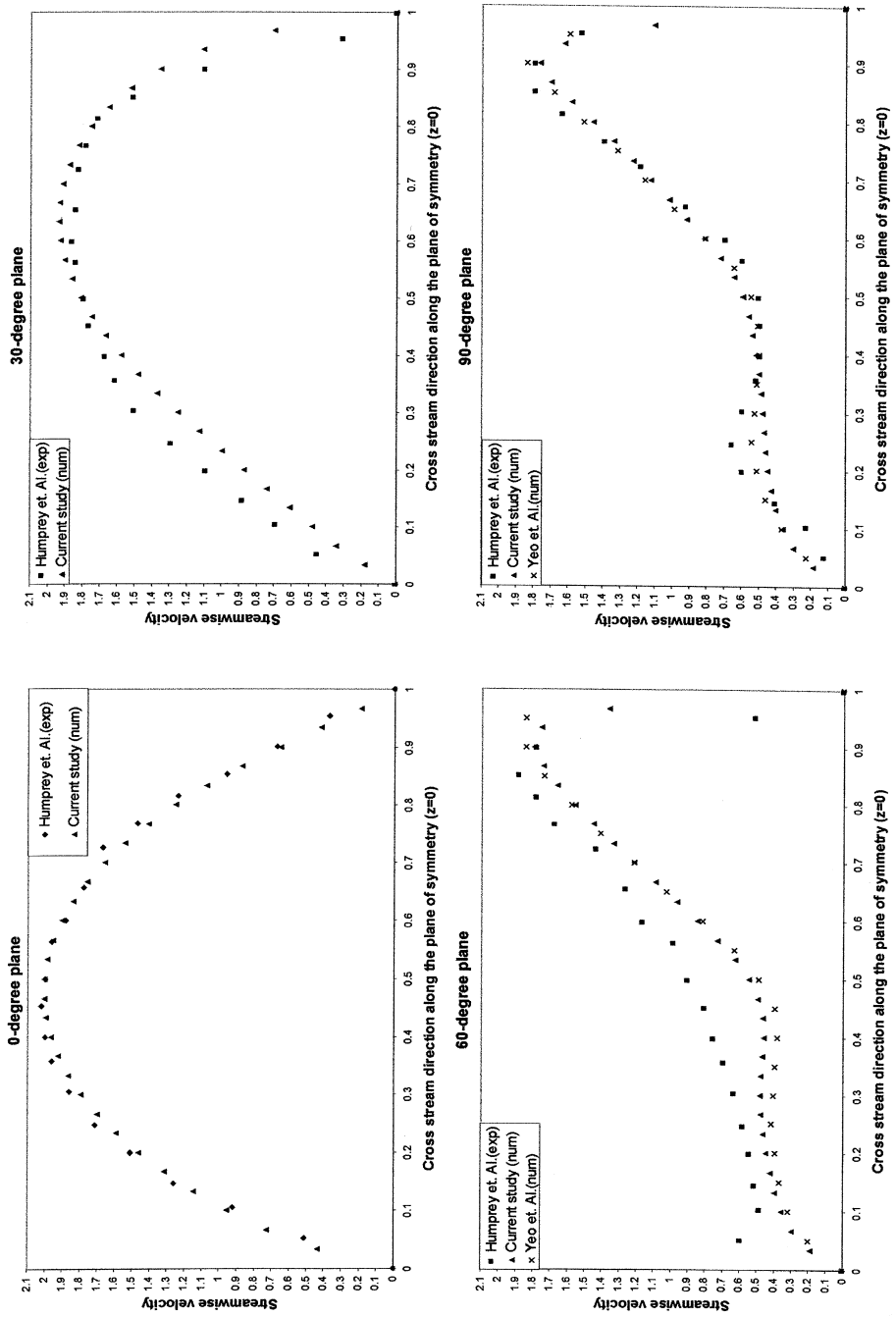

Figure 2.
Velocity profiles at various angular streamwise locations with square cross-section (Re = 790, Ro = 0.0)

Richardson extrapolation analysis with grid doubling, as suggested by Roache (1998), was used for the coarse mesh ($51 \times 21 \times 21$). For this mesh, ($51 \times 21 \times 21$), a maximum error estimate of 2.57 percent was obtained for the entire parameter range covered in this work.

Strong curvature in a duct will generate secondary flow. Figure 3 shows secondary flows at different angular locations along the duct. Figures 3(a) and 3(c) show the results for a square duct with a Reynolds number of 790 and a Rossby number of 0.4 at 45° and 90°, respectively. These results are compared with those at the same Reynolds number without rotation, Figures 3(b) and 3(d). The symmetrical secondary flow cells along the centerline in the non-rotating case are due to the strong curvature of the bend. However, in the rotating case there is a lack of cell symmetry due to the Coriolis force.

The flow characteristics differ for a rotating duct with a 90° bend when compared to the non-rotating case. Figure 4 shows variations of the axial velocity profile at the same Reynolds number (Re = 790), but different Rossby numbers. The results are shown at three different angular locations along the bend. No variations were found at 0°, which is due to the fact that at this location the Coriolis force cannot induce secondary flow if the density is constant. The

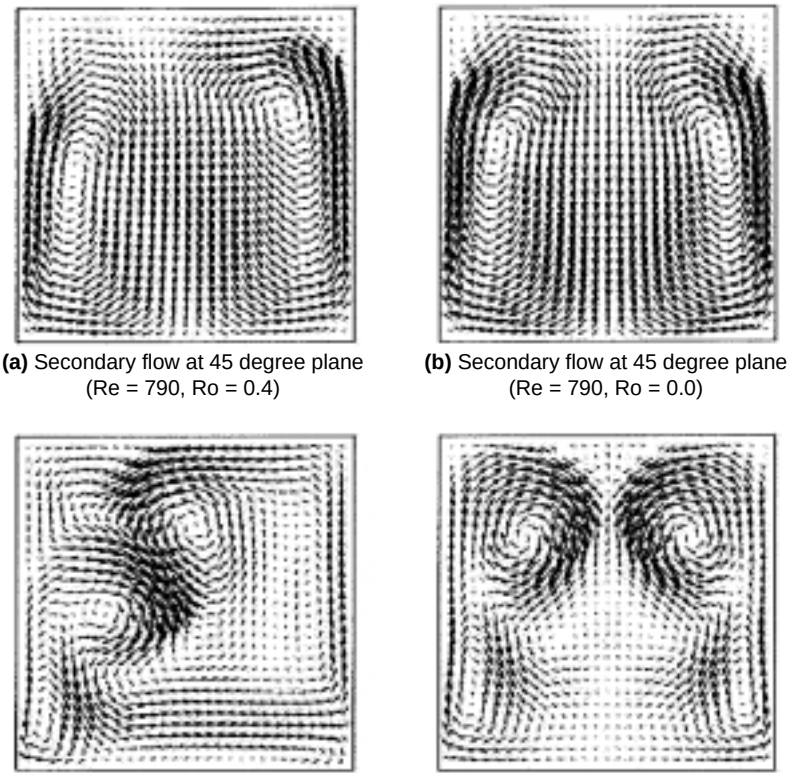

(a) Secondary flow at 45 degree plane (Re = 790, Ro = 0.4)

(b) Secondary flow at 45 degree plane (Re = 790, Ro = 0.0)

(c) Secondary flow at 90 degree plane (Re = 790, Ro = 0.4)

(d) Secondary flow at 90 degree plane (Re = 790, Ro = 0.0)

Figure 3.
Secondary flow vector plot in a rotating and non-rotating 90° bend with square cross-section

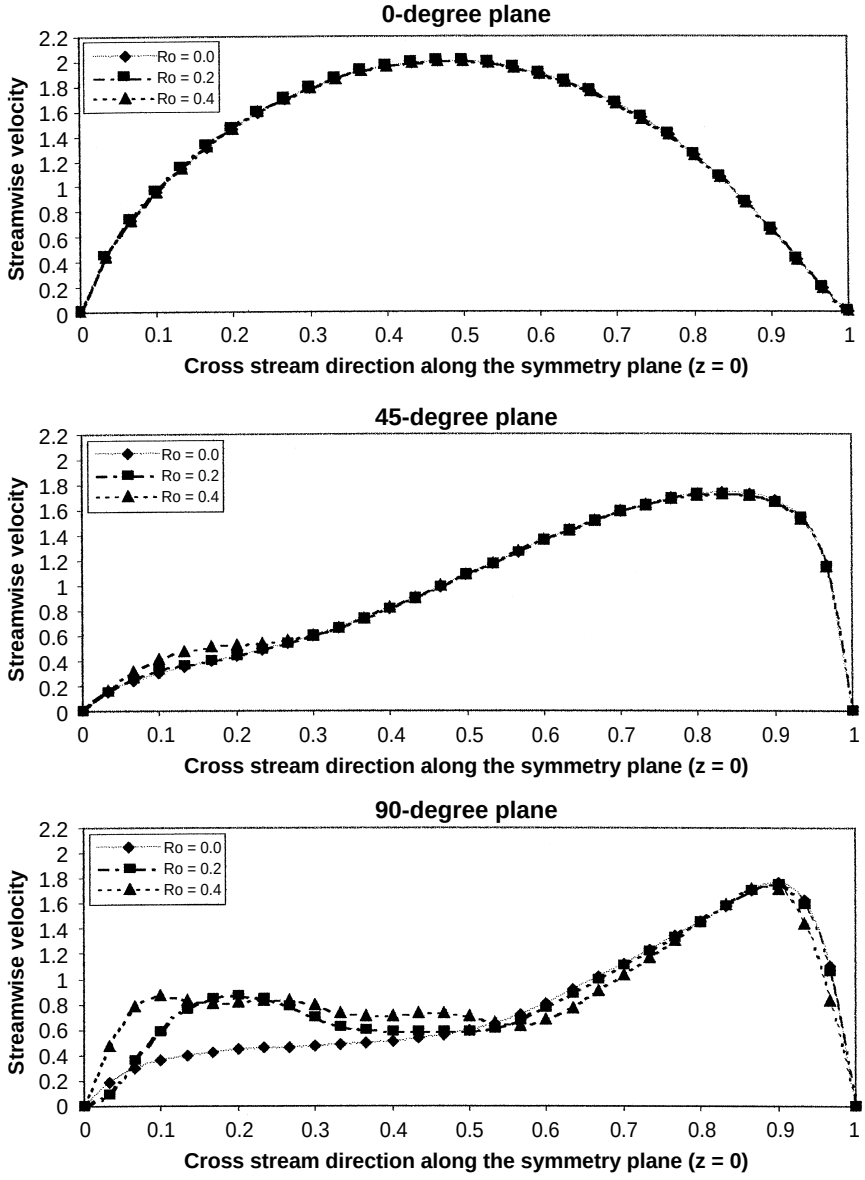

Figure 4.
Axial velocity profile at various angular streamwise locations in a square duct with 90° bend (Re = 790)

flow close to the inner wall of the bend is higher when the Rossby number is increased (higher rotation rate), as can be seen for the 45° and 90° locations. Increasing Rossby number means that Coriolis force effects will increase, and therefore the flow characteristics will differ from the non-rotating case.

Figure 5 shows the velocity and pressure profiles in a 90° bend with a circular cross-section. The results illustrate differences for the rotating and

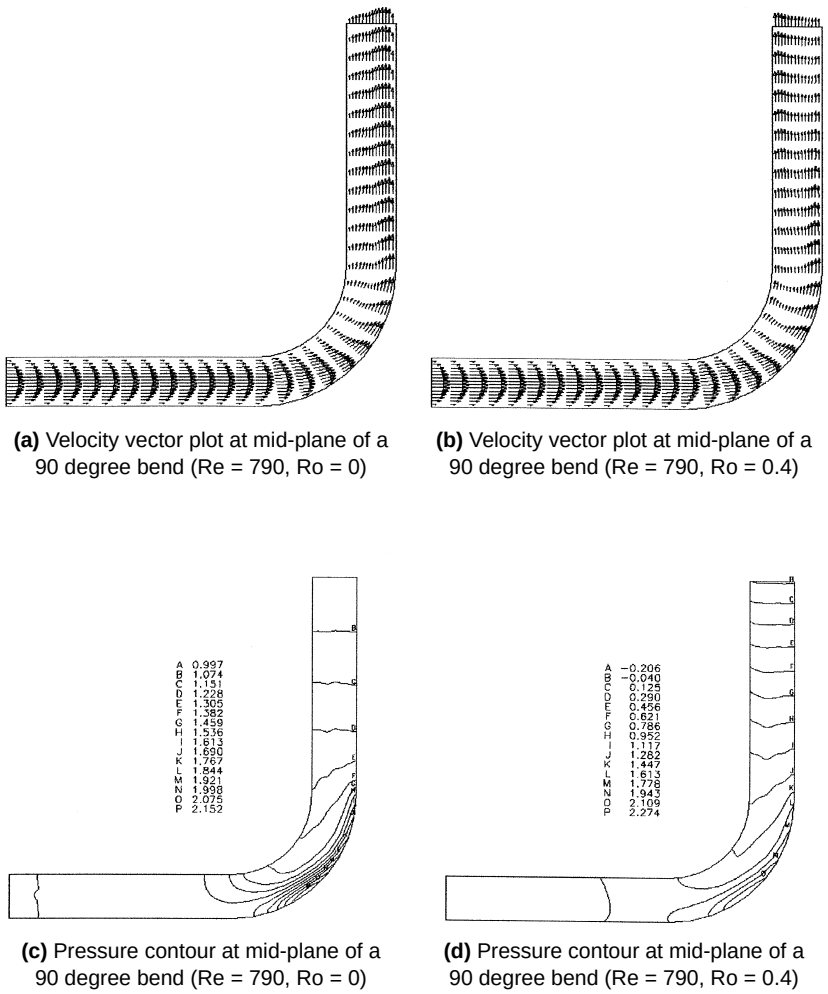

(a) Velocity vector plot at mid-plane of a 90 degree bend (Re = 790, Ro = 0)

(b) Velocity vector plot at mid-plane of a 90 degree bend (Re = 790, Ro = 0.4)

(c) Pressure contour at mid-plane of a 90 degree bend (Re = 790, Ro = 0)

(d) Pressure contour at mid-plane of a 90 degree bend (Re = 790, Ro = 0.4)

Figure 5.
Velocity and pressure plot in a 90° bend with circular cross-section at different Rossby numbers

non-rotating cases. The axial flow along the bend is pushed towards the outer wall for both cases (rotating and non-rotating), see Figures 5(a) and 5(b). However, the axial flow at the outlet will be pushed towards the inner wall for the rotating case. Figures 5(c) and 5(d) show the pressure contours for both cases.

Figure 6 compares the axial velocity profiles at the 90° plane at different Rossby numbers for the circular and square ducts with a Reynolds number of 790. The Coriolis forces push the flow towards the inner wall of the bend for both the square and circular ducts. The strong curvature pushes the flow towards the outer wall. Therefore, two regions with high flow are obtained at the inner wall and the outer wall of the bend for Ro = 0.4 in a square or circular duct, and the rotation mainly affects the flow near the inner wall.

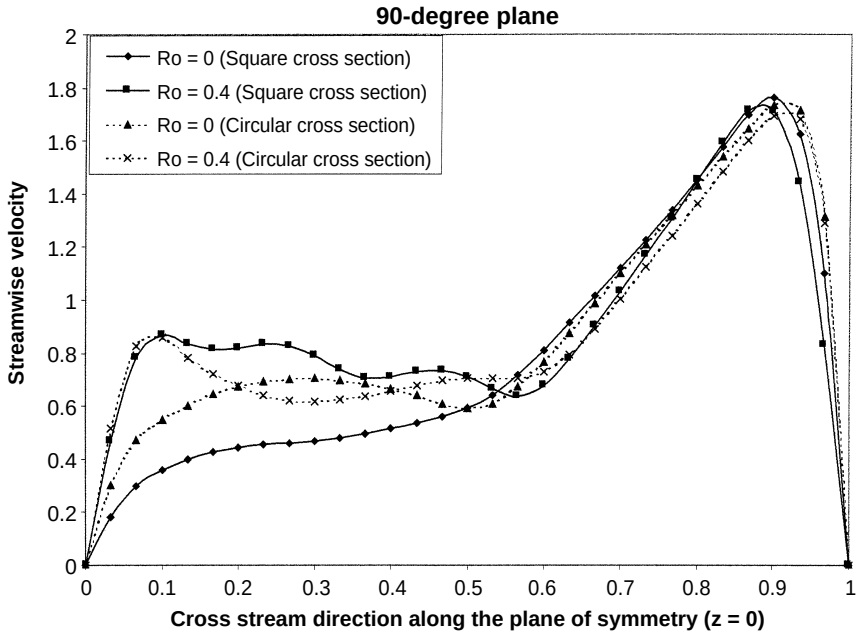

Figure 6.
Axial velocity profile at 90° plane along the symmetry plane with square and circular cross-section (Re = 790)

Secondary flow in a 90° bend with a circular cross-section is shown in Figure 7. For the non-rotating case or zero Rossby number, it can be seen that there is formation of two symmetrical vortex cells at the 45° plane and the formation of four symmetrical vortex cells at the 90° plane. The secondary flow was not symmetrical for the rotating cases. This behavior agrees with that obtained previously for the square duct (Figure 3).

The friction losses in a rotating 90° bend are the result of the wall-friction effects in the inlet and outlet straight sections and the losses due to the bend. In this work is shown the rotation effect on the wall friction factor and the 90° bend losses for the channel with square cross-section. Similar behavior is expected for the 90° bend with circular cross-section under rotation.

Because of the difference in mode of rotation for the inlet and outlet straight sections, the friction factors in these two sections are different. Figure 8 shows the effects of the Rossby number and Reynolds number on axial variation of (f•Re), which is used to express the friction performance of the straight channels. The values taken on each straight section are spanwise averages. The straight dashed line on this figure represents the result for fully developed laminar flow in a straight stationary channel, (f•Re) = 14.2. As can be seen from Figure 8, the friction factor at the straight inlet section is similar to the one obtained for a square duct without rotation, and it increases only close to the bend. This result was expected because the inlet section is in parallel rotation mode and the fluid density is assumed constant; therefore the Coriolis force will not affect the flow.

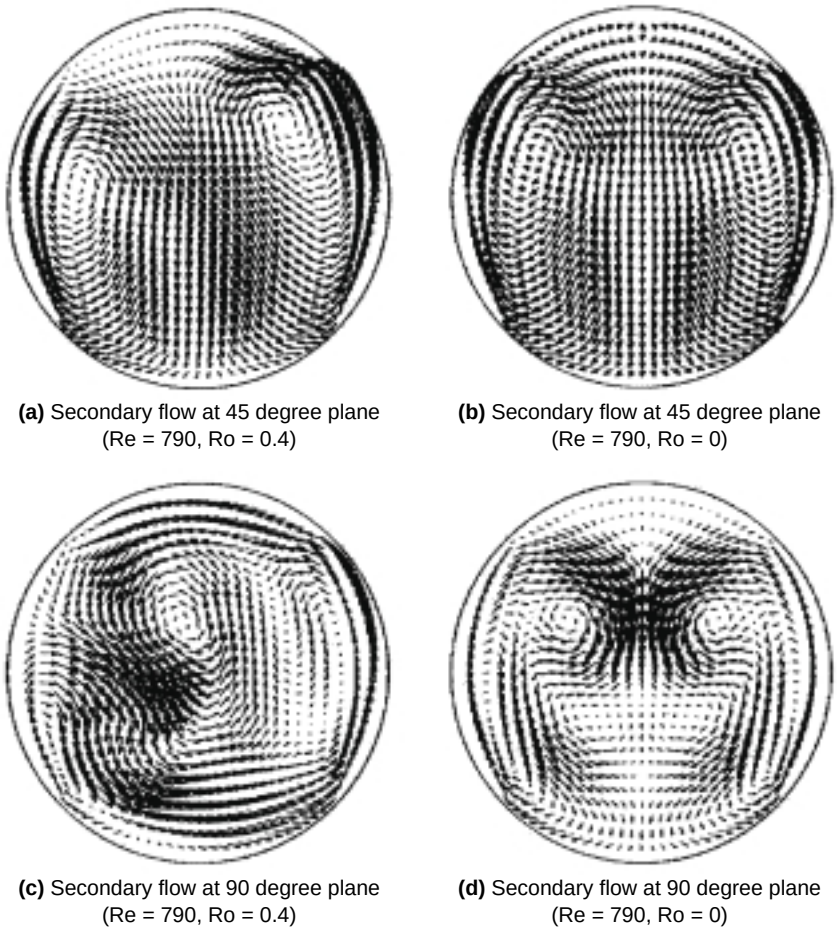

(a) Secondary flow at 45 degree plane (Re = 790, Ro = 0.4)

(b) Secondary flow at 45 degree plane (Re = 790, Ro = 0)

(c) Secondary flow at 90 degree plane (Re = 790, Ro = 0.4)

(d) Secondary flow at 90 degree plane (Re = 790, Ro = 0)

Figure 7.
Secondary flow vector plot in a 90° bend with circular cross-section at different Rossby numbers

Figure 9 shows the wall friction factor for the outlet straight section in a 90° bend with a square cross-section. The results are shown at different Reynolds and Rossby numbers. The values obtained in this section are higher than those obtained for the inlet straight section. The friction factor is higher in this section because of the secondary flows due to the strong curvature of the bend and the Coriolis force.

The pressure drop due to the bend is specified by the loss coefficient, K_T, which is defined as $K_T = (P_{ent.} - P_{ex.})/2$, where $P_{ent.}$ and $P_{ex.}$ are the dimensionless stagnation pressures at the entrance and exit planes of the 90° bend, respectively. Figure 10 gives the Rossby number dependence of the loss coefficient of the bend for two Reynolds numbers, 790 and 500. The loss coefficient decreases with increasing Reynolds numbers for both stationary and rotating conditions. However, the loss coefficient increased with increasing

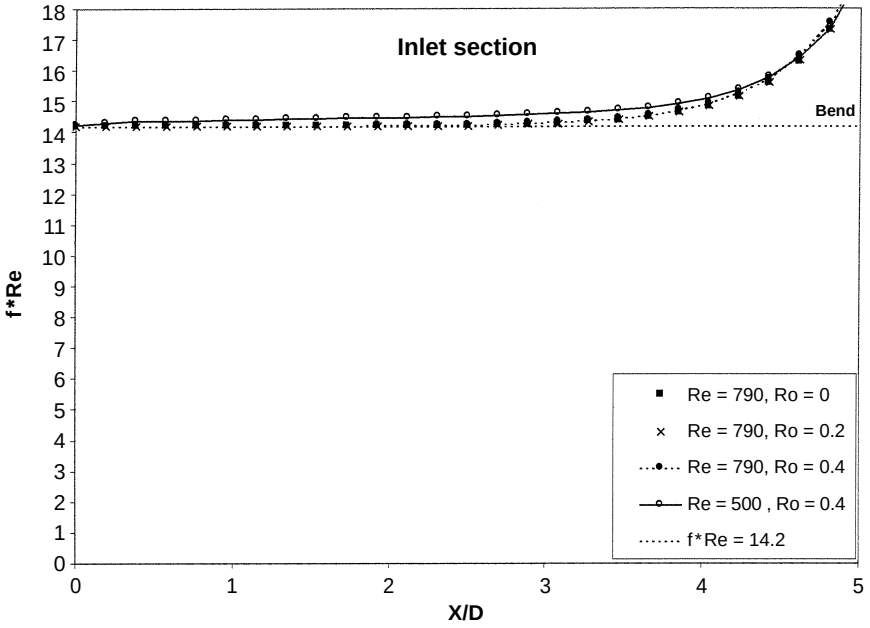

Figure 8.
Friction factor at the inlet section for a 90° bend with square cross-section

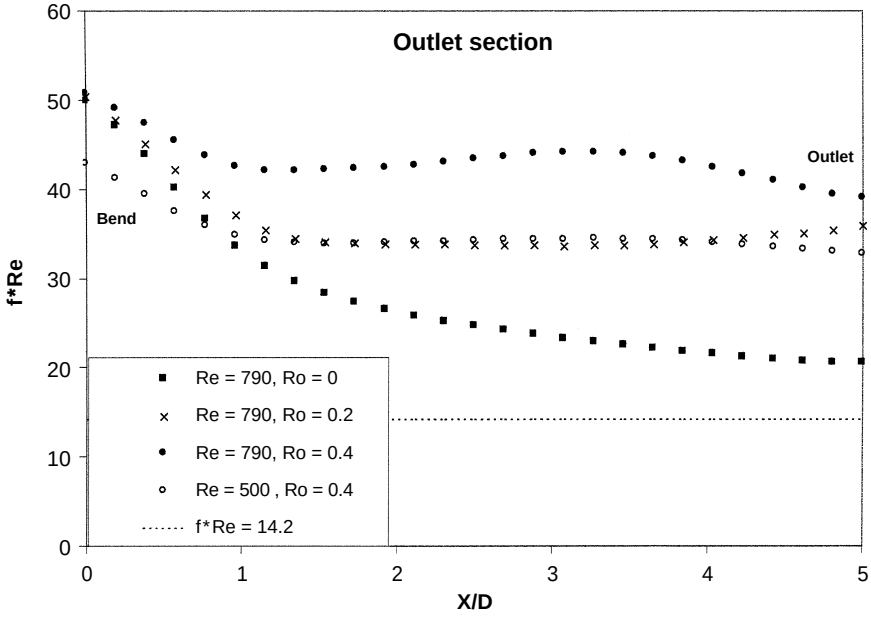

Figure 9.
Friction factor at the outlet section for a 90° bend with square cross-section

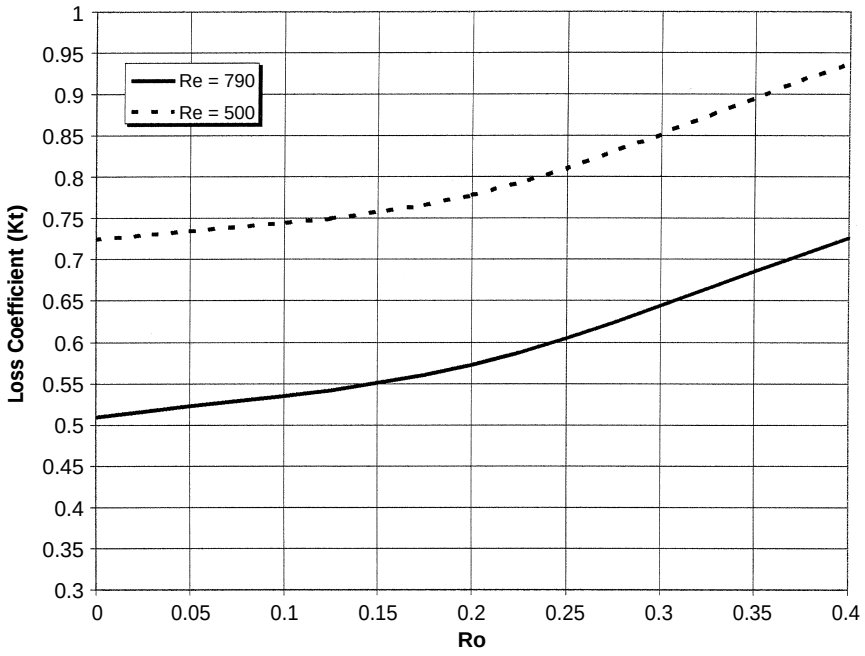

Figure 10.
Rossby number dependence of loss coefficient in the 90° bend with square cross-section

Rossby number because the secondary flow due to the bend curvature is enhanced with rotation. Hwang and Lai (1998) reported that the loss coefficient decreased with increasing Rossby number for the flow in a 180° sharp turn. It should be noted that these authors neglected the centripetal term in the transverse direction. These terms have been shown to be important in both directions in the vicinity of the bend.

Conclusions

An analysis has been presented for studying three-dimensional laminar viscous flows in rotating ducts with strong curvature. The governing equations were successfully solved using the artificial compressibility method. The results obtained allow us better to understand the flow characteristics occurring inside rotating ducts.

Solutions have been presented at different Reynolds and Rossby numbers in circular or square ducts. The present work considers the flow to be laminar. Important variations were found in these results when the Rossby number was increased. Coriolis forces can significantly alter secondary flow due to strong curvatures. The numerical study reassures us that rotation enhances secondary flow and will affect the axial flow.

In this work it was found that friction factors increase dramatically in the outlet straight section after the 90° bend if the duct is rotating. Also, the pressure drop in a 90° bend will increase with rotation. These two factors

should be taken into account in the design of cooling systems in blades. Further investigations are needed to better understand flow characteristics under rotation in complex geometries.

References

Barua, S.N. (1955), "Secondary flow in a rotating straight pipe", *Proc. Roy. A*, Vol. 227, pp. 133-9.

Benton, G.S. and Boyer, D. (1966), "Flow through a rapidly rotating conduit of arbitrary cross-section", *J. Fluid Mech.*, Vol. 26 No. 1, pp. 69-79.

Chen, K.H. (1990), "A primitive variable, strongly implicit calculation procedure for two and three-dimensional unsteady viscous flows. Applications to compressible and incompressible flows including flows with free surfaces", *Doctoral Dissertation*, Iowa State University, Ames, IA.

Chorin, A.J. (1967), "A numerical method for solving incompressible viscous flow problems", *J. Comp. Phys.*, Vol. 2, pp. 12-26.

Hill, P.G. and Moon, I.M. (1962), "Effects of Coriolis forces on the turbulent boundary layer in rotating machines", Report No. 69, Gas Turbine Laboratory, Massachusetts Institute of Technology, Cambridge, MA.

Humphrey, J.A.C., Taylor, A.M.K. and Whitelaw, J.H. (1977),"Laminar flow in a square duct of strong curvature", *J. Fluid Mech.*, Vol. 83 No. 3, pp. 509-27.

Hwang, J. and Lai, D. (1998), "Three-dimensional laminar flow in a rotating multiple-pass square channel with sharp 180 degree turns", *ASME J. Fluid Eng.*, Vol. 120, pp. 488-95.

Ito, H. and Nanbu, K. (1971), "Flow in rotating straight pipes of circular cross section", *ASME J. Basic Eng.*, Vol. 93 No. 3, pp. 383-94.

Johnston, J.P., Halleen, R.M. and Lezius, D.K. (1972), "Effects of spanwise rotation on the structure of two-dimensional fully developed turbulent channel flow", *J. Fluid Mech.*, Vol. 56 No. 3, pp. 533-57.

Moore, J. (1967), "Effects of Coriolis forces on turbulent flow in rotating channels", Report No, 89, Gas Turbine Laboratory, Massachusetts Institute of Technology, Cambridge, NJ.

Moore, J. (1973), "A wake and an eddy in a rotating radial flow passage. Part 1: experimental observations", ASME Paper No.73-GT-57, presented at the ASME Gas Turbine Conference, Washington, DC, April.

Mori, Y. and Nakayama, W. (1968), "Convective heat transfer in a rotating radial circular pipes. 1st report, laminar region)", *Int. J. Heat Mass Transfer*, Vol. 11, pp. 1025-40.

Roache, P.J. (1998), *Verification and Validation in Computational Science and Engineering*, Hermosa Publishers, Albuquerque, NM.

Vaidyanathan, K. (1998), "Coupled strongly implicit Navier-Stokes computation using artificial compressibility formulation for incompressible internal flow problems", Doctoral dissertation, University of Toledo, Toledo, OH.

Viviand, H. (1974), "Conservation forms of gas dynamics equations", *Rech. Aerosp.*, No. 1974-1, pp. 65-8.

Yeo, R.W., Wood, P.E. and Hrymak, A.N. (1991), "A numerical study of laminar 90 degree bend duct flow with different discretization schemes", *ASME J. Fluid Eng*, Vol. 113, pp. 563-8.